Letters

IOP Publishing

Journal of Physics: Condensed Matter

J. Phys.: Condens. Matter **30** (2018) 32LT02 (6pp)

https://doi.org/10.1088/1361-648X/aad022

Letter

Photo-induced lattice contraction in layered materials

Hiroyuki Kumazoe[1], Aravind Krishnamoorthy[2], Lindsay Bassman[2], Rajiv K Kalia[2], Aiichiro Nakano[2], Fuyuki Shimojo[1] and Priya Vashishta[2]

[1] Department of Physics, Kumamoto University, Kumamoto 860-8555, Japan
[2] Collaboratory for Advanced Computing and Simulations, University of Southern California, Los Angeles, CA 90089-0242, United States of America

E-mail: anakano@usc.edu and shimojo@kumamoto-u.ac.jp

Received 26 April 2018, revised 21 June 2018
Accepted for publication 29 June 2018
Published 16 July 2018

Abstract

Structural and electronic changes induced by optical excitation is a promising technique for functionalization of 2D crystals. Characterizing the effect of excited electronic states on the in-plane covalent bonding network as well as the relatively weaker out-of-plane dispersion interactions is necessary to tune photo-response in these highly anisotropic crystal structures. In-plane atom dynamics was measured using pump-probe experiments and characterized using *ab initio* simulations, but the effect of electronic excitation on weak out-of-plane van der Waals bonds is less well-studied. We use non-adiabatic quantum molecular dynamics to investigate atomic motion in photoexcited MoS_2 bilayers. We observe a strong athermal reduction in the lattice parameter along the out-of-plane direction within 100 fs after electronic excitation, resulting from redistribution of electrons to excited states that have lesser anti-bonding character between layers. This non-trivial behavior of weakly bonded interactions during photoexcitation could have potential applications for modulating properties in materials systems containing non-covalent interactions like layered materials and polymers.

Keywords: MoS_2, photo-dynamics, van der Waals, layered materials, quantum molecular dynamics

(Some figures may appear in colour only in the online journal)

1. Introduction

2D transition metal dichalcogenides (TMDC) and vertical van der Waals heterostructures [1] are emerging functional materials for applications involving ultra-responsive photodetection [2], valleytronics [3], photonics and transistors for nanoelectronics [4–6]. Optical and electronic excitation is a promising method for modulating electronic structure and properties of these 2D materials [7, 8], complementing more traditional techniques like chemical doping [9] and intercalation [10], thermal treatment [8, 11] and lattice strain [12]. In-plane lattice dynamics in graphene and other layered materials like TMDCs has been investigated extensively [13–15]. Recent ultrafast electron diffraction experiments and theoretical calculations on these systems have demonstrated softening of specific vibrational modes reflecting a collective distortion of covalent bonds due to mild and moderate electronic excitation [16, 17]. Higher optical intensities and correspondingly greater photogenerated carrier concentrations can cause bond-cleavage or increased reactivity in both bulk and layered materials, which can be utilized for photocatalytic applications [18–21]. While the effect of strong excitation on the covalent network is known, its impact on the crystal structure along the out-of-plane direction dominated by long-range van der Waals forces is only just beginning to be experimentally explored, thanks to the development of electron

sources with femtosecond resolutions [22]. The recent work by Mannebach *et al* provides initial insights in this field, exposing the non-trivial behavior of van der Waals interaction modulated by mild photoexcitation [23]. To better understand this phenomenon, we used non-adiabatic quantum molecular dynamics (NAQMD) to model atomic motion in photoexcited MoS_2 bilayers.

2. Results

The impact of instantaneous photoexcitation on the crystal structure along the non-covalently-bonded direction is quantified through the separation between MoS_2 monolayers, c, at different times after excitation. This inter-layer distance is equal to the vertical (i.e. out of plane) separation between atoms in each MoS_2 monolayer in the simulation cell. Interplanar distance reflects the time-dependent response of atoms to deformations in the energy landscape of the excited crystal and can help in understanding and tuning ionic motion along the non-covalently-bonded directions. Figure 1(a) depicts the MoS_2 bilayer crystal in the 2H structure. At time $t < 0$, prior to photoexcitation, the two MoS_2 layers are separated by 6.228 Å, equal to the out-of-plane lattice parameter obtained from a zero-Kelvin density functional theory (DFT) calculation. Electronic excitation due to optical irradiation is modeled by modifying the occupancy of Kohn–Sham electronic energy levels at $t = 0$, which are then propagated in time using time-dependent density functional theory (TDDFT). Figure 1(b) depicts the evolution of Kohn–Sham eigenlevels and their occupancies when 6 electrons are excited from the Valence Band of the MoS_2 bilayer crystal to the Conduction Band. At $t = 125$ fs, non-adiabatic electron dynamics is simulated through surface hopping., as detailed in the Methods section.

The time-dependent inter-layer separation in photoexcited bilayers for various excited charge carrier densities is shown in figure 2(a), along with the calculated inter-layer distance in an unexcited bilayer crystal in an adiabatic molecular dynamics (AMD) simulation for comparison. The measured c-axis lattice constant along the adiabatic MD simulation at 10 K increases from the 0 K DFT value of 6.228 Å to over 6.240 Å, which is consistent with the expected thermal expansion of the lattice in going from 0 K to 10 K. However, the lattice constant measured in our NAQMD simulation of photoexcited systems show an unexpected non-thermal contraction of ≈0.02 Å for excited charge carrier densities above 2×10^{21} cm^{-3}. Figure 2(b) shows the evolution of inter-layer separation in NAQMD simulations relative to values obtained from the unexcited adiabatic MD simulations, indicating that lattice contraction effect becomes stronger with increasing excitation and excited charge carrier density. Similar lattice contraction was observed experimentally in photoexcited MoS_2 multilayers, which were attributed to stronger van der Waals interactions in the excited state induced by changes in atomic polarizability by redistribution of electron densities [23].

However, it is important to note that our simulations are performed at charge carrier densities around 10^{21} cm^{-3} which lie in the electron–hole plasma regime and are three orders of magnitude greater than charge carrier densities of 10^{18} cm^{-3} probed in experiments, which lie firmly in the regime of excitonic physics [23]. As a result, the magnitude ($\eta_c = -3.2 \times 10^{-3}$ in our simulations against -7×10^{-4} in their experiments) as well as time period ($\tau \sim 0.2$ ps in our simulations against ~100 ps in experiments) of inter-layer strain observed in these simulations differs greatly from experiments. Both differences point to the existence of a different mechanism for the rapid and strong inter-layer response of MoS_2 in NAQMD data. In order to understand the mechanism responsible for the lattice contraction, we investigate the origin of forces on atoms in our NAQMD simulations.

3. Discussion

To understand the origin of the unexpected layer contraction, we decompose the total Hellmann–Feynman forces on each MoS_2 layer, $\boldsymbol{F}_{\text{tot}}$, into two components, $\boldsymbol{F}_{\text{att}}$, the attractive part and $\boldsymbol{F}_{\text{rep}}$, the repulsive component. $\boldsymbol{F}_{\text{att}}$ includes all forces which lead to greater bonding between the two layers and a reduction in inter-layer separation. $\boldsymbol{F}_{\text{rep}}$ is the summation of all forces that lead to an increase in inter-layer distance.

$$\boldsymbol{F}_{\text{att}} = \boldsymbol{F}_{\text{non-local}} + \boldsymbol{F}_{\text{PCC}} + \boldsymbol{F}_{\text{DFT-D}}, \quad (1)$$

$$\boldsymbol{F}_{\text{rep}} = \boldsymbol{F}_{\text{coulomb}} + \boldsymbol{F}_{\text{local}}. \quad (2)$$

In equation (1), $\boldsymbol{F}_{\text{non-local}}$ and $\boldsymbol{F}_{\text{PCC}}$ are the average forces on all atoms in a single MoS_2 layer due to the non-local part of the pseudopotential and partial core corrections respectively. $\boldsymbol{F}_{\text{DFT-D}}$ is the average van der Waals force on the atoms, computed using the DFT-D2 method of Grimme [24].

Figure 3(a) shows the calculated values of $\boldsymbol{F}_{\text{att}}$ at $t = 0$ for the MoS_2 bilayer as a function of electronic excitation. Attractive forces on the MoS_2 layers increases to 69 meV Å^{-1} for excited charge carrier concentrations beyond 0.67×10^{21} cm^{-3} from a value of 21 meV Å^{-1} in the unexcited ground state. Interlayer van der Waals forces, calculated through the DFT-D method, which is insensitive to the distribution of electronic charge density in the system, remains constant at all values of electronic excitation (figure 3(b)). This approximation is not inconsistent with previous reports of modulation of van der Waals forces due to optical excitation, since these effects occur on timescales two orders of magnitude larger than those investigated in this study.

Instead, we have found that this large contraction in lattice constant can be ascribed to variations in the magnitude of wave function overlap across the inter-layer van der Waals space. This direct bonding interaction can be quantified through analysis of bond overlap populations (BOP). Here, the Kohn–Sham eigenstates are projected on to atomic orbital basis centered at each atomic position. Mulliken BOP are then calculated as the sum of overlap integrals for all pair of atoms

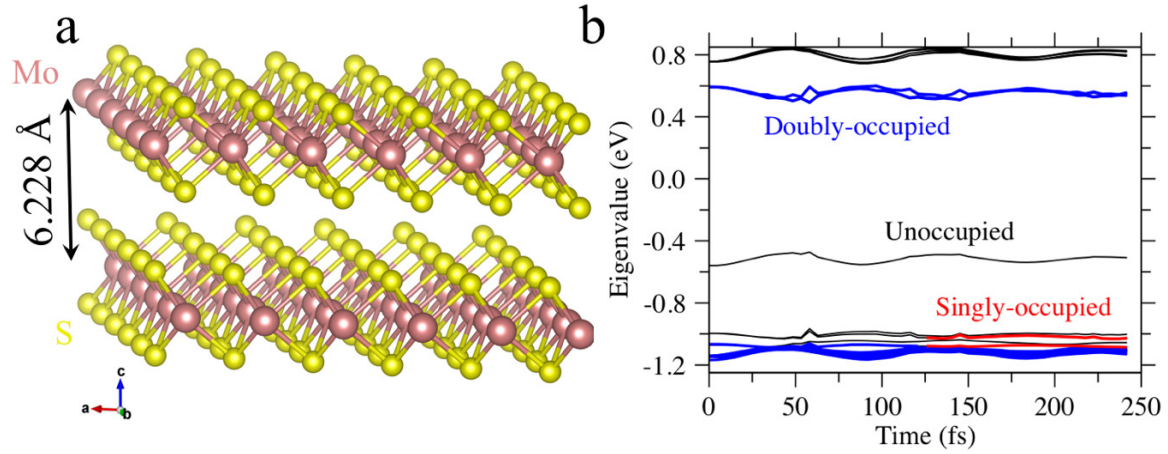

Figure 1. (a) Bilayer MoS_2 crystal containing $6 \times 6 \times 1$ unit cells, used as the initial configuration for adiabatic and non-adiabatic molecular dynamics simulations. Here, sulfur and molybdenum are depicted as yellow and brown spheres. (b) Eigenlevels near the Fermi energy in a simulation with a very large excited carrier density of 3.5×10^{21} cm^{-3} electrons. Unoccupied, singly occupied and doubly-occupied energy levels are indicated by color coding. Switching of level occupancies is simulated by surface hopping, indicated by the transition at $t = 125$ fs.

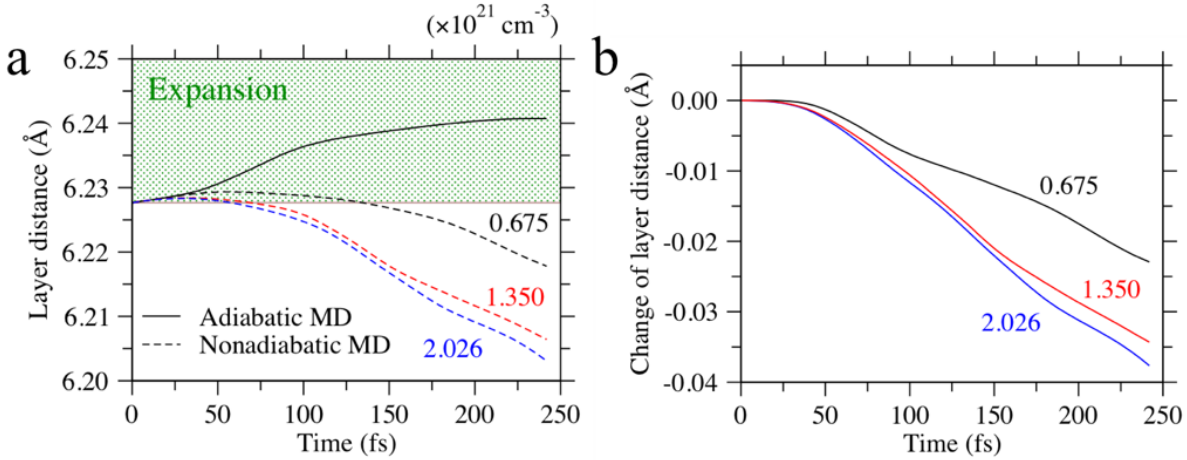

Figure 2. (a) Calculated inter-layer distance, $d_{AMD}(t)$ for the MoS_2 bilayer increases monotonically in the absence of electronic excitation (solid line). In contrast, the inter-layer separation in NAQMD simulations, $d_{NAMD}(t)$ shows a non-thermal contraction with time. (b) Time evolution of change of inter-layer separation in NAQMD simulations, relative to the adiabatic case, i.e. $d_{AMD}(t) - d_{NAMD}(t)$, shows more pronounced lattice contraction with increasing charge carrier concentration.

across the van der Waals gap [25]. Figure 3(c) shows the band-decomposed BOP for all atom pairs across the van der Waals gap in the ground state. The highest occupied valence energy level, the valence band maximum (VBM) corresponds to a highly negative value of BOP and represents strong anti-bonding interaction along the c-axis. This quantification is supported by the presence of a nodal plane along the c-axis (figure 3(d)). In contrast, the four degenerate unoccupied energy levels from the conduction band minimum (CBM) to CBM + 3 are localized on a single layer within the simulation cell, and therefore do not contribute to bonding along the c-axis. Here, CBM + n denotes the nth energy level above CBM. Lower energy states from VBM − 3 to VBM − 1 are delocalized over both MoS_2 layers and contribute to a finite, positive value of BOP and a corresponding small attractive force between layers. Here, VBM − n denotes the nth energy level below CBM.

Moderate electronic excitation from the VBM to CBM (corresponding to an overall excited charge carrier density of n(e–h) $= 0.67 \times 10^{21}$ cm^{-3}) leads to the depopulation of the strongly antibonding and repulsive VBM state and the population of the non-bonding CBM state leading to a net increase in the attraction between MoS_2 layers. Subsequent excitation (e.g. VBM − 1 to CBM + 1) involves promoting electrons from the mildly bonding occupied state to the non-bonding CBM states, which does not significantly change the attractive interaction, consistent with the flattening of the attractive force $\boldsymbol{F}_{att}$ (figure 3(a)) for charge carrier concentrations beyond 0.7×10^{21} cm^{-3}.

In addition to thee attractive forces, electronic excitation also modulates the overall repulsive interaction between layers. As equation (2) suggests, the total repulsive interaction between layers has two components, $\boldsymbol{F}_{local}$, the average force on all atoms in a single MoS_2 layer due to the local part of

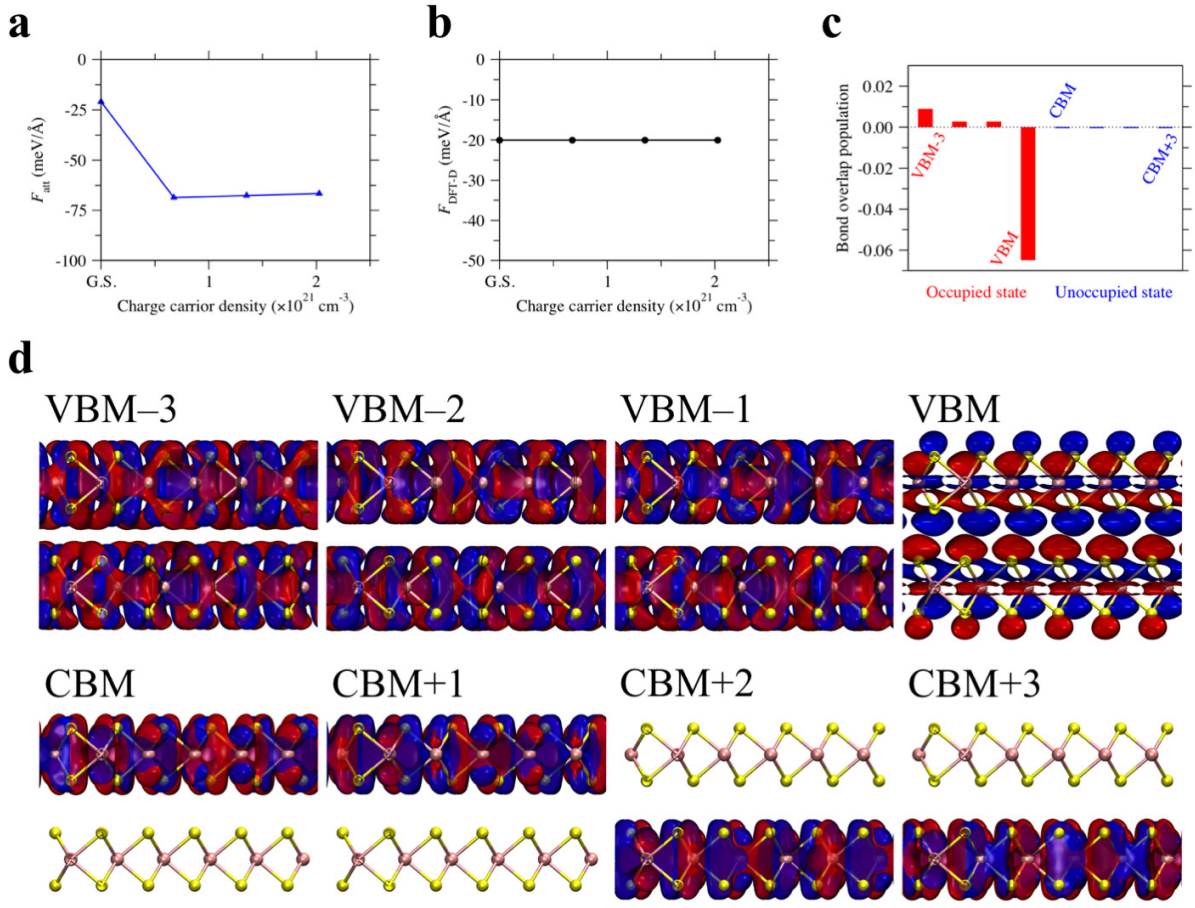

Figure 3. (a) The z-component of the average attractive force per atom in the MoS_2 bilayer system as a function of charge carrier density. On the vertical axis, a negative value corresponds to an attractive force. (b) Average van der Waals force per atom of the MoS_2 bilayer, computed using the DFT-D method remains constant with charge carrier concentration, and is therefore not responsible for the increase attraction observed in the excited state. (c) Bond overlap population between layers as a function of band. (d) A snapshot of positive (blue) and negative (red) ground-state quasi-wavefunction of energy states near the Fermi level. Contour surfaces are drawn at $\pm$ 3.5 $\times$ 10^{-3} a.u.$^{-3/2}$.

the pseudopotential and $\boldsymbol{F}_{\text{Coulomb}}$, the average multipolar Coulomb interaction between the charge densities of each MoS_2 layer. Figure 4(a) shows the variation of the overall repulsive force, $\boldsymbol{F}_{\text{rep}}$ as a function of electronic excitation, showing that repulsive forces increase sharply from a moderate value of 20.9 meV Å^{-1} to 68.6 meV Å^{-1} with initial excitation of 0.67 $\times$ 10^{21} cm^{-3}. This sharp increase in repulsive interactions is dominated by variations in the Coulombic interaction. To understand the source of this interaction, we plot the planar-averaged electronic charge density (over the x-y plane) of the excited bilayer relative to planar averaged density in the ground state (figures 4(b)–(d)). These figures show that charge redistribution due to electronic excitation leads to the accumulation of negative charge in the interlaminar region, leaving the MoS_2 layers positively charged.

The charge redistribution profiles in figure 4(b) also provide qualitative insight into the nature of Coulombic interaction between the photoexcited layers. The symmetric nature of the charge redistribution implies that there is no net charge transfer between layers during photoexcitation. This lack of charge transfer precludes the existence of monopole-monopole Coulomb interactions between layers. Instead, redistribution of electron density from the MoS_2 layers to the interlaminar region due to moderate photoexcitation (0.67 $\times$ 10^{21} cm^{-3}) leads to the formation of two electric dipoles, one at each MoS_2 layer, between the positive charge on the layer and the negative charge at the interlaminar region. The repulsive interaction between these two oppositely-oriented dipoles constitutes the majority of the Coulomb interaction in figure 4. Subsequent photoexcitation (greater than 1.3 $\times$ 10^{21} cm^{-3}) leads only to charge distribution from to both sides of the MoS_2 layer, which does not significantly change the induced dipole moment or the repulsive Coulombic interaction.

Figure 5(a) summarizes the attractive, repulsive and total force on the MoS_2 bilayer system as a function of excited charge carrier concentration and shows the sharp increase in both attractive and repulsive interactions with excitation (to 0.67 $\times$ 10^{21} cm^{-3}). Figure 5(b) shows only the total force on a MoS_2 layer (equal to the sum of the attractive and repulsive forces acting on it) clearly indicating that the increase in attractive interactions is incompletely balanced by the repulsive interactions, leading to a net negative (i.e. attractive) force between

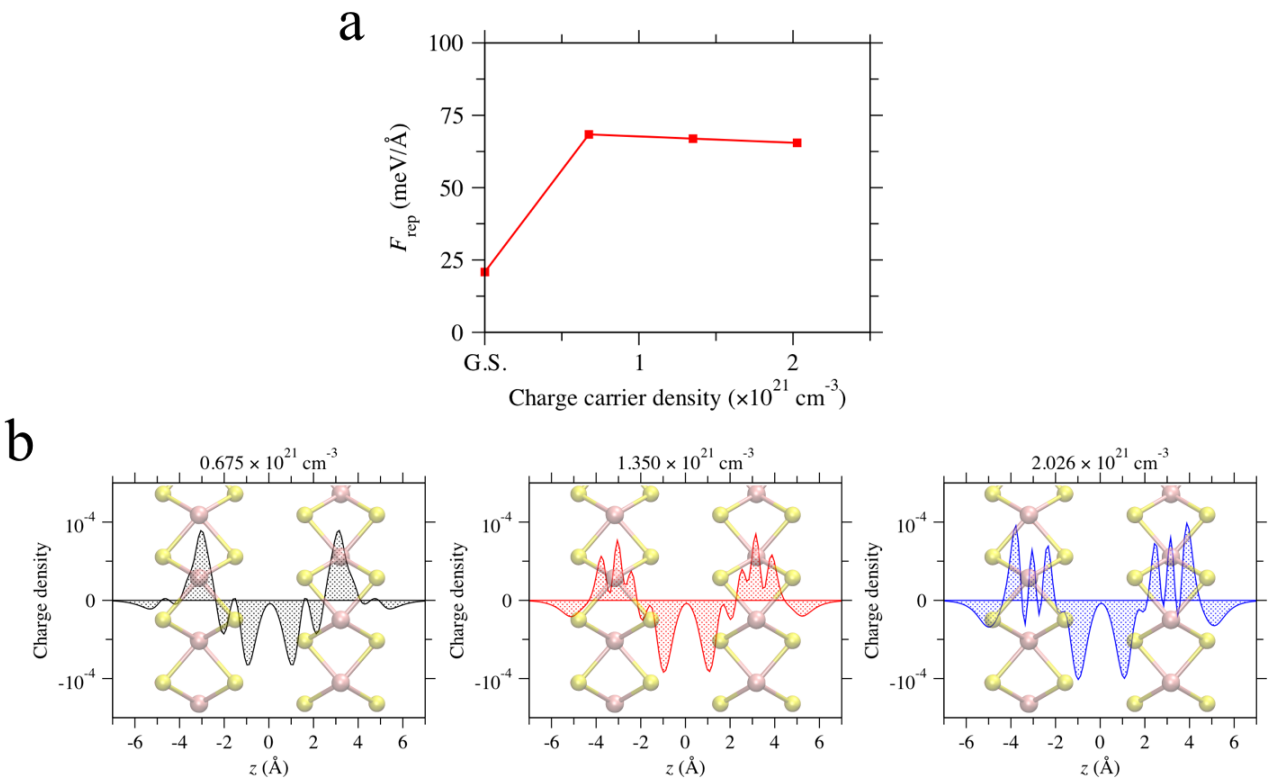

Figure 4. (a) The z-component of the average repulsive force per atom in the MoS_2 bilayer system as a function of charge carrier density. On the vertical axis, a positive value corresponds to a repulsive interaction. (b) Planar-average of charge redistribution in the excited state, relative to the ground state, for excited charge carrier densities of 0.67 × 10^{21} cm^{-3}, 1.35 × 10^{21} cm^{-3}, and 2.03 × 10^{21} cm^{-3} respectively.

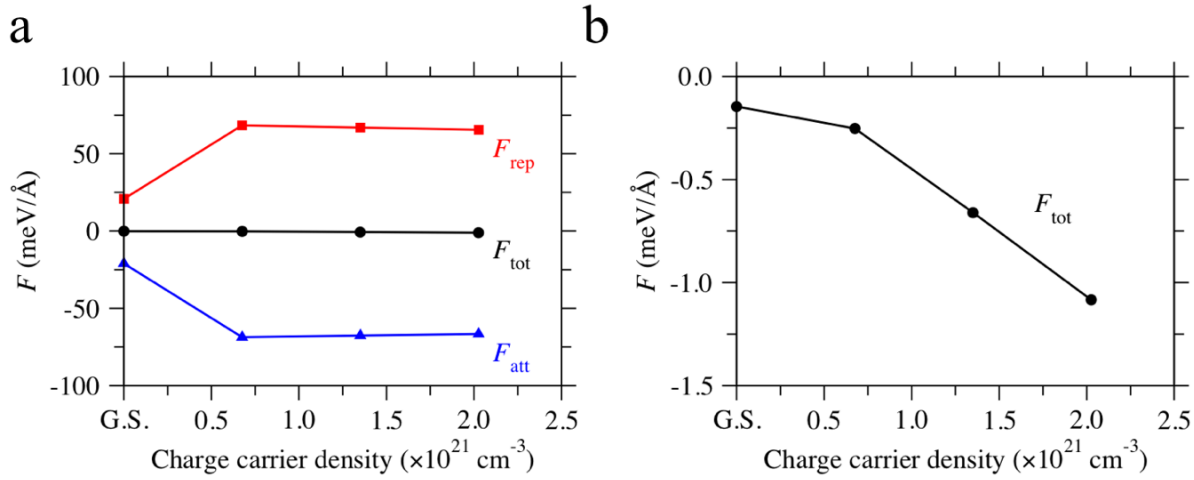

Figure 5. (a) The z-component of the attractive, repulsive and total force between two layers in the MoS_2 bilayer as a function of total charge carrier density. (b) Total force between layers as a function of excitation. Incomplete cancellation of attractive and repulsive forces results in a net attractive force that increases with increasing charge carrier density.

the MoS_2 layers. This imbalance between attractive and repulsive components increases with charge carrier density, leading to a net attractive force on the MoS_2 layers that increases from 0.2 meV $Å^{-1}$ in the unexcited state (which falls within the convergence threshold for the current DFT simulations) to over 1 meV $Å^{-1}$ for large excited charge carrier densities.

4. Conclusion

In summary, we have modeled changes in the out-of-plane lattice parameter in a model layered material, bilayer MoS_2, using NAQMD simulations. Our simulations show a strong and rapid reduction of the out-of-plane lattice constant

($\eta_c = -3.2 \times 10^{-3}$ and $\tau = 0.2$ ps) upon electronic excitation. The instantaneous electronic excitation leads to a large spatial redistribution of electron density away from interlaminar regions to towards the MoS_2 layers. This redistribution increases both the attractive and repulsive interaction between layers, by respectively strengthening the out-of-plane overlap between MoS_2 wave functions and repulsive dipole interactions between layers. An incomplete cancellation of these competing forces leads to a small attractive interaction between layers, leading to the observed lattice contraction in the out-of-plane direction.

5. Simulation methods

Adiabatic electronic structure is calculated using DFT and the projector-augmented-wave method [26]. Exchange-correlation energy is approximated with the generalized gradient approximation (GGA) framework [27]. Electron charge density and wave-functions are respectively described using Fourier components up to 240 Ry and 30 Ry. Van der Waals interactions between atoms are estimated using the semi-empirical DFT-D approximation and all structures are relaxed till the total force on each atom in the simulation cell is below 1.6 meV $Å^{-1}$ [24]. The reciprocal space is sampled using Γ point in the Brillouin zone. The simulation cell consists of 72 atoms of Mo and 144 S atoms and spans $19.14 \times 19.14 \times 22.34$ $Å^3$. NAQMD follows the trajectories of all atoms, while describing electronic excitations and nonadiabatic transitions between excited electronic states assisted by atomic motions based on TD-DFT and surface-hopping approaches, thereby describing photoexcitation dynamics involving electrons and nuclei [28]. To perform large NAQMD simulations involving many hundreds of atoms, we have implemented a series of techniques for efficiently calculating long-range exact exchange correction and excited-state forces. Details of our QMD and NAQMD simulation software are described in [29]. All NAQMD simulations were performed in the NVT ensemble at 10 K. Reference adiabatic MD simulations for the unexcited bilayer are performed by coupling the simulation cell to a Nosé-Hoover thermostat at 10 K. Adiabatic MD simulations are performed with a step size of 4.84 fs.

Acknowledgments

This work was supported as part of the Computational Materials Sciences Program funded by the US Department of Energy, Office of Science, Basic Energy Sciences, under Award Number DE-SC00014607. The simulations were performed at the Argonne Leadership Computing Facility under the DOE INCITE program and at the Center for High Performance Computing of the University of Southern California.

ORCID iDs

Aravind Krishnamoorthy https://orcid.org/0000-0001-6778-2471

References

[1] Geim A K and Grigorieva I V 2013 *Nature* **499** 419–25
[2] Wang H N, Zhang C J, Chan W M, Tiwari S and Rana F 2015 *Nat. Commun.* **6** 8831
[3] Schaibley J R, Yu H Y, Clark G, Rivera P, Ross J S, Seyler K L, Yao W and Xu X D 2016 *Nat. Rev. Mater.* **1** 16055
[4] Wang Q H, Kalantar-Zadeh K, Kis A, Coleman J N and Strano M S 2012 *Nat. Nanotechnol.* **7** 699–712
[5] Manzeli S, Ovchinnikov D, Pasquier D, Yazyev O V and Kis A 2017 *Nat. Rev. Mater.* **2** 17033
[6] Liu Y P *et al* 2016 *Nano Lett.* **16** 488–96
[7] Krishnamoorthy A, Bassman L, Kalia R K, Nakano A, Shimojo F and Vashishta P 2018 *Nanoscale* **10** 2742–7
[8] Cho S *et al* 2015 *Science* **349** 625–8
[9] Kochat V *et al* 2017 *Adv. Mater.* **29** 1703754
[10] Voiry D, Mohite A and Chhowalla M 2015 *Chem. Soc. Rev.* **44** 2702–12
[11] Ma Y, Liu B, Zhang A, Chen L, Fathi M, Shen C, Abbas A N, Ge M, Mecklenburg M and Zhou C 2015 *ACS Nano* **9** 7383–91
[12] Song S, Keum D H, Cho S, Perello D, Kim Y and Lee Y H 2016 *Nano Lett.* **2016** 188–93
[13] Kolobov A V, Fons P and Tominaga J 2016 *Phys. Rev.* B **94** 094114
[14] Waldecker L, Bertoni R, Hubener H, Brumme T, Vasileiadis T, Zahn D, Rubio A and Ernstorfer R 2017 *Phys. Rev. Lett.* **119** 036803
[15] Mannebach E M *et al* 2015 *Nano Lett.* **15** 6889–95
[16] Lin M-F *et al* 2017 *Nat. Commun.* **8** 1745
[17] Zeng S M, Zhao Y C, Li G and Ni J 2016 *Phys. Rev.* B **94** 024501
[18] Bealing C R and Ramprasad R 2013 *J. Chem. Phys.* **139** 174904
[19] Liao J M, Sa B S, Zhou J, Ahuja R and Sun Z M 2014 *J. Phys. Chem.* C **118** 17594–9
[20] Kolesov G, Vinichenko D, Tritsaris G A, Friend C M and Kaxiras E 2015 *J. Phys. Chem. Lett.* **6** 1624–7
[21] Bang J, Meng S, Sun Y Y, West D, Wang Z G, Gao F and Zhang S B 2013 *Proc. Natl Acad. Sci. USA* **110** 908–11
[22] Weathersby S P *et al* 2015 *Rev. Sci. Instrum.* **86** 073702
[23] Mannebach E M *et al* 2017 *Nano Lett.* **17** 7761–6
[24] Grimme S, Antony J, Ehrlich S and Krieg H 2010 *J. Chem. Phys.* **132** 154104
[25] Mulliken R S 1955 *J. Chem. Phys.* **23** 1841–6
[26] Hohenberg P and Kohn W 1964 *Phys. Rev.* **136** B864–4
[27] Perdew J P, Burke K and Ernzerhof M 1996 *Phys. Rev. Lett.* **77** 3865–8
[28] Shimojo F, Ohmura S, Mou W W, Kalia R K, Nakano A and Vashishta P 2013 *Comput. Phys. Commun.* **184** 1–8
[29] Shimojo F, Kalia R K, Kunaseth M, Nakano A, Nomura K, Ohmura S, Shimamura K and Vashishta P 2014 *J. Chem. Phys.* **140** 18A529